Introduction

Friedreich's ataxia (FRDA) is a rare, serious, progressive, life-threatening genetic disease caused by a deficiency in frataxin (FXN). It has an incidence that is estimated to be 1:29,000 and a carrier frequency of ~ 1:85 (1). In the US, there are an estimated 4,000 to 5,000 patients with FRDA. The disease leads to neurodegeneration, cardiomyopathy and scoliosis, and presents with a combination of difficulties in walking, muscle weakness, loss of sensation and proprioception, and impaired speech (2). FRDA primarily affects the nervous and cardiac tissues, but others may also be affected, such as pancreatic, ocular and auditory tissues (1). The inheritance pattern of FRDA is autosomal recessive; the underlying genetic mutation found in most patients with FRDA (97%) is a hyperexpansion of a guanosine adenosine adenosine (GAA) triplet repeat in the *FXN* gene (3), posing a transcriptional block that results in a deficiency in the mitochondrial protein FXN. Depending upon the tissue tested and quantification method employed, tissue FXN concentrations in patients with FRDA have been reported to be between 21.1%−32.2% compared to normal healthy volunteer (NHV) control individuals (4). This quantitative deficiency of FXN constitutes the pathophysiological root cause of the disease (5). The degree of FXN deficiency varies among affected individuals, and patients with lower FXN levels experience earlier onset of disease that progresses more rapidly and is more severe (3). Individuals who are heterozygous carriers, typically having mean FXN concentrations at approximately 50%, are phenotypically normal (3, 4).

FXN is a ubiquitously expressed mitochondrial protein (6). It is nuclear encoded, produced in the cytoplasm, and imported into the mitochondria aided by an MTS present at its N-terminus (7, 8). The biological function of FXN is not completely understood; however, it was found to regulate the biogenesis of mitochondrial Fe-S clusters (9). Fe-S clusters are essential components that act as prosthetic groups

✉ Gopi Shankar
gshankar@larimartx.com

[1] Discovery Laboratory, Larimar Therapeutics Inc., King of Prussia, PA, USA

[2] Statistics & Quantitative Sciences, Larimar Therapeutics Inc., Bala Cynwyd, PA, USA

[3] Corporate Office, Larimar Therapeutics Inc., 3 Bala Plaza, Suite 506, Bala Cynwyd, PA 19004, USA

for various mitochondrial enzymes such as aconitase (10) and succinate dehydrogenase (11) that have been found to be functionally impaired in patients with FRDA (12). This impairment in enzyme function is likely due to the deficiency of FXN in patients with FRDA, highlighting the protein's importance in maintaining proper mitochondrial function and energy production.

Nomlabofusp, previously known as CTI-1601 (CAS 2548202–05-5), is being developed by Larimar Therapeutics, Inc., (Bala Cynwyd, PA, USA) as a protein replacement therapy intended to treat the deficiency of endogenous FXN in adults and children with FRDA, thereby addressing the pathophysiological cause of this disease. It is a novel recombinant fusion protein designed to deliver human FXN to the mitochondria. As a 224-amino acid long protein (24.9 kDa), nomlabofusp contains a short, trans-activator of transcription (TAT) sequence-based cationic cell penetrant peptide, fused through a diglycine linker to the amino-terminus of human FXN, which comprises its native mitochondrial targeting sequence (MTS) and mature FXN protein (Fig. 1a). The TAT CPP has been shown to have a broad tissue distribution (13), a feature that is advantageous for the treatment of a genetic disease in which the affected protein is deficient in all tissues, even if in FRDA some tissues are more vulnerable than others (1). The safety, pharmacokinetic, and pharmacodynamic profiles of subcutaneously administered nomlabofusp in single ascending dose (SAD) and multiple ascending dose (MAD) Phase 1 studies in adults with FRDA have been published (14). Patients with FRDA who received nomlabofusp in the MAD were observed to have dose dependent increases in FXN levels in skin and buccal tissues.

Following administration and distribution to tissues, nomlabofusp enters cells and is imported into mitochondria where it is processed, releasing mature FXN. As illustrated in Fig. 1b, the TAT-CPP domain shepherds nomlabofusp through the cell membrane into the cell where the MTS domain enables import through the mitochondrial membranes into the matrix. There it is cleaved by mitochondrial protein peptidase (MPP) (15, 16), producing mature and active human FXN within the mitochondrial matrix – a crucial step in the maturation of FXN, and a process indistinguishable from the transfer and processing of endogenous FXN. The increased level of mature FXN (mFXN) is thereby expected to restore downstream effects such as the activation of iron-sulfur cluster dependent enzymes (17) and potentially other pharmacodynamic effects representing the homeostatic regulatory functions of FXN.

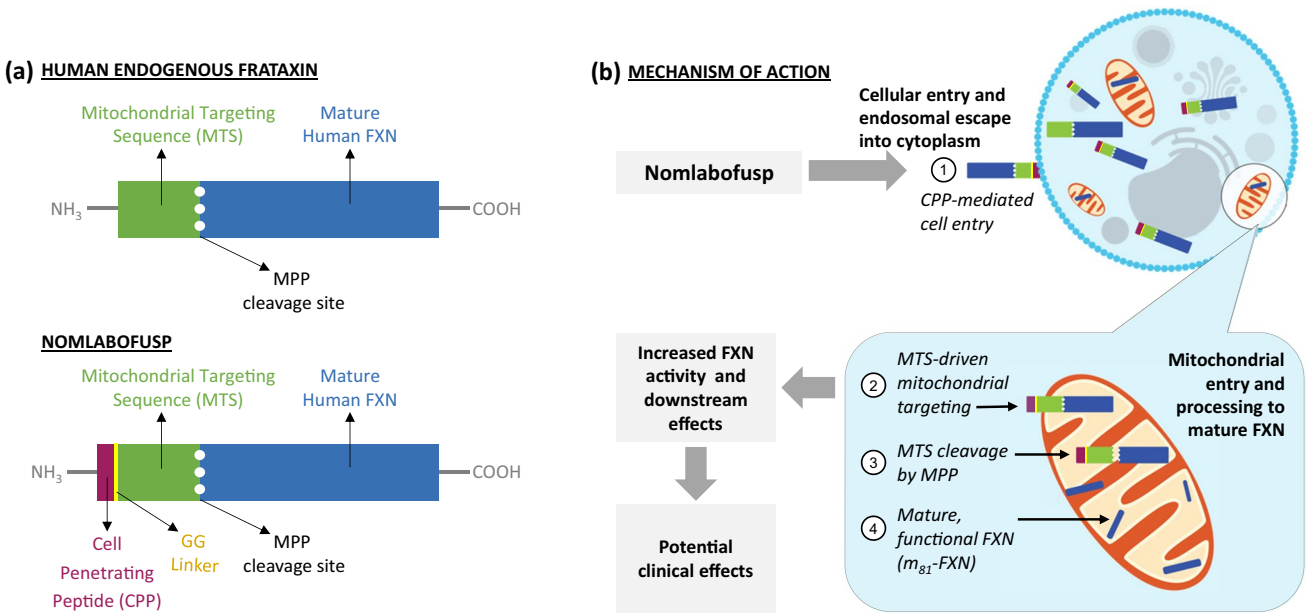

Fig. 1 Structure and proposed mechanism of action of nomlabofusp. (**a**) Nomlabofusp is a recombinant fusion protein consisting of an N-terminal cell penetrant peptide (CPP) fused through a diglycine (Gly-Gly) linker to the amino terminus of the complete human frataxin molecule (FXN), comprising the mitochondrial targeting sequence (MTS) and mature frataxin protein (mFXN). The CPP amino acid sequence contains a methionine start followed by the trans-activator of transcription (TAT) protein transduction domain sequence, YGRKKRRQRRR. The fusion protein maintains the mitochondrial processing peptidase (MPP) cleavage site between the MTS and mFXN present in endogenous human frataxin; this allows for the CPP and MTS to be cleaved by MPP to produce mature human frataxin in the mitochondria. (**b**) With the aid of its cell-penetrant peptide (CPP) nomlabofusp enters a cell, where its mitochondrial targeting sequence (MTS) allows the molecule to be imported into mitochondria. Following import into the mitochondrial matrix, the MTS is removed proteolytically by the mitochondrial processing peptidase (MPP), releasing mature frataxin (mFXN)

In this article we present evidence for the proposed mechanism of action of nomlabofusp, specifically its entry into the cell and subsequently the mitochondria to deliver functional FXN, supporting the use of nomlabofusp as a potential FXN replacement therapy for patients with FRDA. Using cultured cell lines, we demonstrate the cellular entry and mitochondrial localization of nomlabofusp where it is processed into mature human FXN. Additionally, we show that this process occurs in study subjects with FRDA who had been administered nomlabofusp by demonstrating an increase in mature FXN in buccal cells. A trend toward normalization in the expression of several genes was also found in these patients, commensurate with increases in FXN levels, suggesting that the nomlabofusp-delivered mFXN is pharmacodynamically active in the cell.

Materials and Methods

Cell Lines

The rat embryonic cardiac myoblast cell line H9c2(2–1) (#CRL-1446, ATCC, Manassas, VA, USA) and human neuroblast cell line SH-SY5Y (#94030304, Millipore Sigma, Burlington, MA, USA) were grown in complete media [DMEM (#11995–065, Thermo Fisher Scientific, Waltham, MA, USA), 10% fetal bovine serum (FBS) (#100–106, Gemini Bioproducts West Sacramento, CA, USA), 1% antibiotic/antimycotic (#15240–062, Gibco, Waltham, MA, USA)] at 37°C, 5% CO_2. FXN knockdown and scramble controls in mouse myoblast C2C12 cells (#CRL-1772, ATCC) were generated via lentiviral transduction of a lentiviral vector expressing a shRNA targeting mouse FXN (#TL514670V, Origene Technologies, Rockville, MD, USA) or scrambled shRNA (#TR30021V, Origene Technologies). Cells were transduced with lentiviral particles in the presence of 10 mg/mL polybrene (#107689, Millipore Sigma), then selected in complete media with 5 µg/mL puromycin (#A11138-03, Gibco). Knockdown clones were verified via western blot. FXN knockdown and scramble controls in human HEK293 cells (#CRL-1573, ATCC) were similarly generated, except lentiviral particles targeting human FXN (#TL312891V, Origene Technologies) were used, and positive clones were selected using 0.75 µg/mL puromycin.

Nomlabofusp Treatment of Cell Lines

To transduce with nomlabofusp (manufactured by KBI Biopharma Inc., Boulder, CO, USA), media was aspirated, cells were washed twice with phosphate buffered saline (PBS) (#20012–027, Gibco), and transduction media [DMEM, 1% heat-inactivated FBS, 20 mM glycerol (#15514–011, Invitrogen, Waltham, MA, USA)] containing nomlabofusp, or an equal volume of vehicle (20 mM histidine, 250 mM sucrose, 0.5% polysorbate 20, pH 5.8) was added to each well. Cells were incubated for 3 h, then an equal volume of complete media was added to cells. This procedure was repeated approximately 24 and 48 h later, for a total of three treatments. The next day, cells were washed with PBS, treated with TrypLE Express (#12604–021, Gibco) to degrade extracellular nomlabofusp and displace the cells from the plastic surface. TrypLE Express was neutralized with an equal volume of complete media before subsequent analysis.

Cellular Extracts and Mitochondrial Isolation

After nomlabofusp treatment, the cells were collected by centrifugation. For analysis of whole cell extracts, the cell pellet was resuspended in PBS, centrifuged again, and then lysed by resuspension in RIPA buffer (#R0278, Millipore Sigma) supplemented with HALT protease inhibitor and EDTA (#78438, Thermo Fisher Scientific). Lysates were clarified by centrifugation at 21,000 × *g* for 5 min at 4°C, and the supernatant was transferred to a new tube. Protein concentrations were determined using a bicinchoninic acid assay (BCA) protein assay kit (#23225, Thermo Fisher Scientific). For mitochondrial isolation and analysis, mitochondria were isolated using a Mitochondria Isolation Kit for Cultured Cells (ab110171, Abcam, Cambridge, UK), according to the manufacturer's instructions. Briefly, cell pellets were resuspended in reagent A, then Dounce homogenized using 30 strokes. The homogenate was centrifuged at 1000 × *g* for 5 min at 4°C, and the supernatant was saved. The pellet was resuspended in Reagent B, then Dounce homogenized using 30 strokes and centrifuged at 1000 × *g* for 5 min at 4°C. These two supernatants were combined and centrifuged at 14,000 × *g* for 15 min at 4°C. The resulting supernatant ("cytoplasmic fraction") was precipitated using tricarboxylic acid (TCA) and then resuspended in RIPA buffer supplemented with HALT protease inhibitor and EDTA. The pellet ("mitochondrial fraction") was directly resuspended in RIPA buffer supplemented with HALT protease inhibitor and EDTA. Protein concentrations of mitochondrial fractions were determined using a BCA protein assay kit.

Fluorescence Microscopy

After nomlabofusp treatment, cells (25,000 per well) were seeded onto a 96-well imaging plate (#6055302, Revvity, Waltham, MA, USA) coated with fibronectin (#F1141, Millipore Sigma) and allowed to recover for 24 h. Cells were then washed with PBS and fixed using 4% freshly prepared paraformaldehyde (#1570-S, Electron Microscopy Sciences, Hatfield, PA, USA) for 10 min. Cells were washed twice with PBS and incubated in blocking buffer [5% normal goat serum (#5425S, Cell Signaling

Technologies, Danvers, MA, USA), 0.3% TX-100 (#85111 Thermo Fisher Scientific)] for 1 h at room temperature. Mouse anti-FXN (#ab110328, Abcam) and rabbit anti-Tomm20 (#ab78547 Abcam) were diluted 300-fold and 600-fold, respectively, in blocking buffer, added to each well, and incubated overnight at 4°C. The next day, cells were washed 3 × with PBS. Goat anti-mouse AlexaFluor488 (#ab150116 Abcam) and goat anti-rabbit AlexaFluor594 (#ab150077 Abcam) were each diluted 1000-fold in blocking buffer and incubated for 45 min at room temperature. Cells were washed thrice with PBS, then stained with 1.5 µM Hoechst 33342 (#62249 Thermo Fisher Scientific) for 3 min at room temperature before being washed with PBS. Cells were imaged on an Operetta CLS confocal microscope (Revvity).

Immunoblotting

Protein concentrations of cellular lysate samples, determined using a BCA protein assay kit, were diluted to equal concentrations using water, and protein loading buffer (#928–40004, Li-Cor Biosciences, Lincoln, NE, USA) with 2.5% (v/v) β-mercaptoethanol (#M4138, Millipore Sigma) added according to the manufacturer's instructions. Equal volumes of protein extracts were then loaded onto BOLT 12% Bis–Tris gels (#NW00122, Thermo Fisher Scientific) and run in 1 × MES SDS running buffer (#B0002, Invitrogen) at 130 V for approximately 45 min. Proteins were transferred onto a nitrocellulose membrane using the iBlot2 (#IB23002 Thermo Fisher Scientific) at 20 V for 60 s, 23 V for 90 s, then 25 V for 35 s. Membranes were blocked in Intercept blocking buffer (#927–60001, Li-Cor Biosciences) for 45 – 60 min at room temperature. For primary antibody incubations, mouse anti-FXN (#ab110328, Abcam) and rabbit anti-Tomm20 (#ab78547, Abcam) were diluted in Intercept T20 antibody diluent (#927–65001, LiCor Biosciences) 300-fold and 2000-fold, respectively, and incubated on the membranes overnight at 4°C. Mouse anti-GAPDH (#60,004–1-Ig, Proteintech, Rosemont, IL, USA) and rabbit anti-β-actin (# 8457S, Cell Signaling Technologies) were diluted in Intercept T20 antibody diluent 10,000-fold and incubated for 60 min at room temperature. The membranes were washed thrice with TBST [(#J640 Avantor, Radnor, PA, USA) with 0.1% Tween-20 (#003005, Thermo Fisher Scientific), then incubated with goat anti-mouse 800CW (#925–32210, Li-Cor Biosciences) and goat anti-rabbit 680LT (#925–68071, Li-Cor Biosciences) secondary antibodies diluted 10,000-fold in Intercept T20 antibody diluent for 60 min at room temperature. Membranes were washed thrice with TBST, then imaged using an Odyssey CLx (Li-Cor Biosciences).

Buccal Tissue Samples from Patients with FRDA

Buccal swab tissue samples were obtained from 3 study subjects with FRDA from a study cohort who received 100 mg nomlabofusp via subcutaneous injection daily for 13 days in a Phase 1, double-blind, placebo-controlled MAD study of nomlabofusp (NCT04519567). Samples had been stored at −80°C until used. The study's design and evaluation of safety, pharmacokinetics, and pharmacodynamics after short term nomlabofusp administration were recently published (14). For the immunoprecipitation and western blot experiment, samples from subjects in the 100 mg dose cohort was selected because it involved the maximum duration of daily dosing (13 days) and the median gain in FXN levels (compared with baseline pre-study levels measured in skin and buccal tissues, as measured by the hybrid LC–MS/MS assay described below) were higher than in the 2 lower dose cohorts (25 mg and 50 mg). Only 3 of 7 subjects from the 100 mg cohort were selected because they (a) had both pre-treatment baseline (Day −2) and post-last dose (Day 13) samples available for the intended comparison, and (b) had adequate buccal tissue protein extract volumes available. The 3 subjects' samples from each of the 2 timepoints were combined (i.e., a pooled pre-treatment Day −2 sample and a pooled post-treatment Day 13 sample) because the cellular extract sample volumes were inadequate for testing individually.

FXN Quantification in Buccal Cells

A validated hybrid LC–MS/MS assay was used for FXN quantification in buccal tissue (collected via cheek swabbing), as described previously (14). Briefly, buccal tissue samples (previously stored at −80°C) were homogenized in the presence of a protease inhibitor cocktail (#P8340, Millipore Sigma). Total protein was quantified in the buccal cell homogenates using a BCA protein assay kit. To measure FXN, an immunoaffinity purification extraction step was conducted with an anti-FXN mouse monoclonal antibody (#ab110328, Abcam), enriched proteins were digested to peptides using Trypsin Gold (V5280, Promega, Madison, WI, USA]) and the SGT peptide (SGTLGHPGSLDETTYER, located at the N-terminus of mature human FXN), was quantified by liquid chromatography coupled with tandem mass spectrometry (Shimadzu Nexera X2 UHPLC system coupled with a Sciex API 6500 + mass spectrometer, Framingham, MA). Nomlabofusp with stable isotope-labeled amino acids was used as the internal standard. FXN concentration was reported as a ratio of total cellular protein concentration, in pg/µg units.

FXN Immunoprecipitation and Western Blot Analysis

An anti-FXN antibody (#ab110328, Abcam) was biotinylated using the EZ-Link Sulfo-NHS-LC-Biotin kit (#A39257 Thermo Fisher Scientific). Streptavidin beads (#68817 Thermo Fisher Scientific) were blocked for 1 h at room temperature with Intercept blocking buffer, washed and then incubated with the biotinylated antibody for 1 h at room temperature. Conjugated beads were then washed thrice with PBS to eliminate unbound antibody. Next, 100 µg cell homogenate (from buccal samples of patients with FRDA or a NHV) or nomlabofusp alone were diluted to 500µL in PBS, added to 50µL conjugated beads, and incubated for 3 h at room temperature. Subsequently, the beads were washed thrice with PBS and then eluted with 1x sample loading buffer with 2.5% (v/v) β-mercaptoethanol. Samples were analyzed by immunoblotting as described above, except rabbit anti-FXN (#ab219414, Abcam) was used at a 500-fold dilution as the primary antibody, and goat anti-rabbit 800CW (#926–32211, Li-Cor Biosciences) was used at a 10,000-fold dilution as the secondary antibody. Densitometry measurements were conducted using ImageStudio Lite software (Li-Cor Biosciences).

Gene Expression Analysis

Buccal tissue samples were collected using Puritan DNA/RNA Shield™ swabs (#R1107E, Zymo Research, Irvine, CA, USA). RNA was extracted from samples from patients with FRDA or NHVs using a Chemagic 360 automated RNA extraction system (Revvity) with the chemagic 360 RNA Blood 2.5 k Kit H24 (CMG1084, Revvity). Purified RNA was quantified using a Nanodrop Lite spectrophotometer (Thermo Fisher Scientific). RNA was hybridized to a custom nCounter codeset (Nanostring Technologies, Seattle, WA, USA) for 18 h at 65°C, applied to an nCounter cartridge using an nCounter Prep Station model 5 s (Nanostring Technologies) and read using an nCounter Digital Analyzer model 5 s (Nanostring Technologies) according to the manufacturer's specifications. Technical quality control evaluation was performed for linearity, imaging, limit of detection (LOD), and binding density according to the Gene Expression Data Analysis Guidelines (Nanostring Technologies). The following housekeeping genes were used for normalization: ACTB, ATP6V0C, ESAM, ITPR3, VPS28. Given a per-sample LOD defined as the mean of the counts of the negative control probes for a given sample, quality control evaluations were also performed to identify samples with (a) high proportions of endogenous genes below the per-sample LOD by identifying samples with a higher percent of endogenous genes below the per-sample LOD than the 75th percentile of the distribution of percent below per-sample LOD in the reference group where the reference group is defined as the samples with all housekeeping genes above the per-sample LOD and (b) high proportions of housekeeping genes below the LOD by identifying samples with at least than one housekeeping gene below the per-sample LOD. Normalization was performed using RUVseq by performing upper quartile normalization (18) and then normalization via RUVg (19). Resulting counts were log2 transformed.

Results

Exposure of Cell Lines with Nomlabofusp Leads to Cellular Entry and Increased FXN Levels in Mitochondria

To demonstrate that exogenously added nomlabofusp can translocate into cells growing in culture and be delivered to mitochondria, rat H9c2 cells were exposed to 10 µM nomlabofusp for 3 h over 3 consecutive days. After exposure, the cells were treated with trypsin (TrypLE Express) to degrade non-internalized nomlabofusp and then seeded onto an imaging plate for immunofluorescence staining and visualization. Staining with an antibody specific for human FXN, which does not cross-react with endogenous rat FXN, showed that immunoreactive human FXN (processed mature FXN or nomlabofusp) not only entered the cells but colocalized with the mitochondrial marker Tomm20, suggesting mitochondrial entry (Fig. 2a). As expected, based on the mechanism of cellular entry by TAT-fusion proteins (20–22) and the behavior of TAT itself (23, 24), human FXN staining was also present in punctate structures, presumed to be endosomes, and the nucleus.

Nomlabofusp, comprised of human FXN, its endogenous MTS and TAT, migrates between 25–30 kDa by SDS-PAGE, whereas the fully processed mFXN form is ~ 14 kDa in size. Western blot analysis of rat H9c2 cells after nomlabofusp exposure showed the appearance of the ~ 14 kDa mature human FXN (Fig. 2b), suggesting that nomlabofusp is processed by MPP in the mitochondrial matrix. Further, subcellular fractionation of nomlabofusp treated cells confirmed that the ~ 14 kDa FXN band was present in the mitochondrial fraction (Fig. 2b), demonstrating that nomlabofusp exposure increases levels of human frataxin within mitochondria. Similar results were observed after treating human SH-SY5Y cells with nomlabofusp; FXN signal increased in SH-SY5Y cells after nomlabofusp exposure as measured by immunofluorescence microscopy (Fig. 2c). Using acquisition settings where the endogenous human FXN signal was barely detectable in the vehicle treated cells, FXN signal increased after nomlabofusp exposure, with a partial colocalization to mitochondria. Like the experiment in H9c2 cells, mature FXN levels increased in SH-SY5Y cells

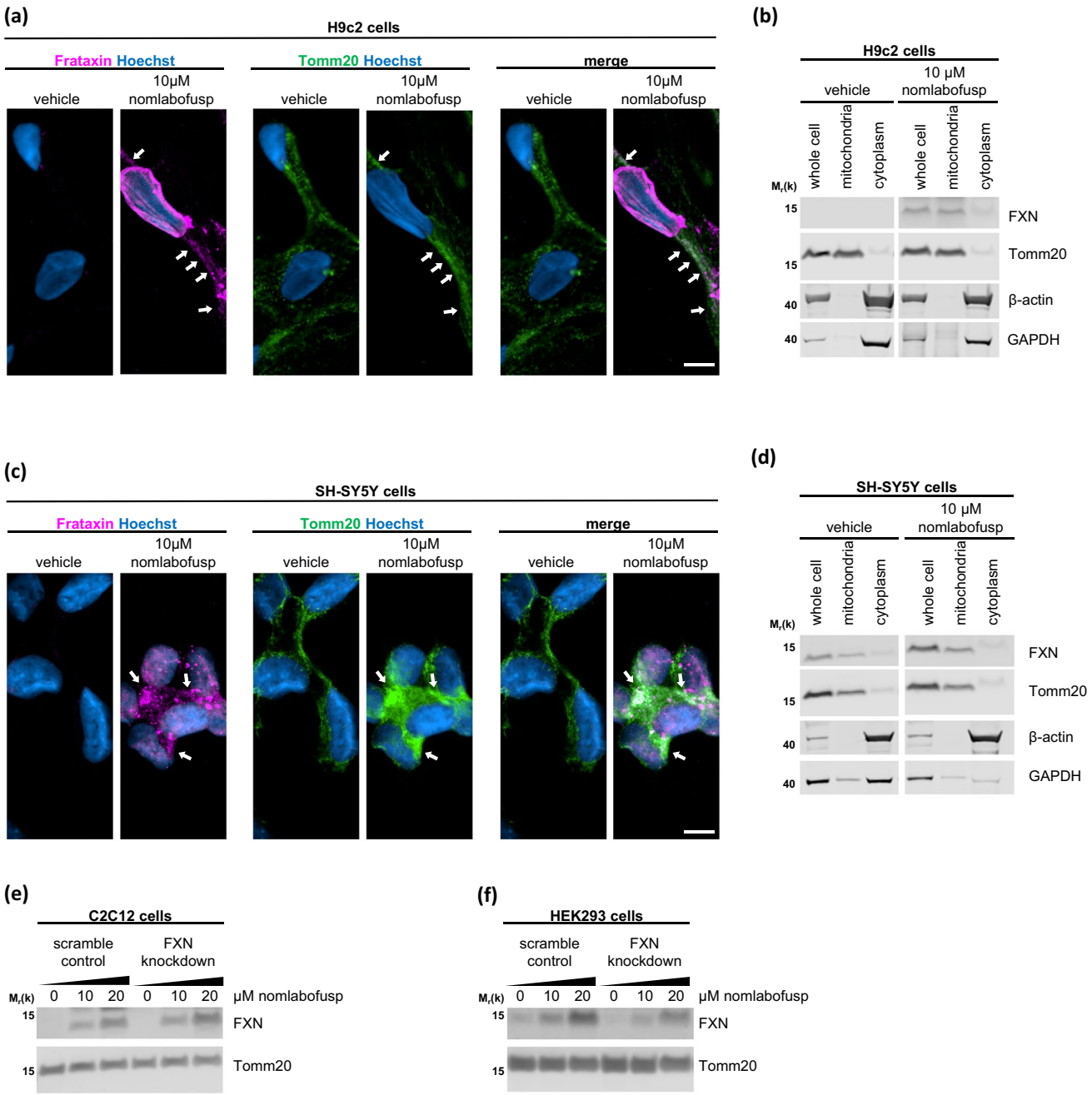

Fig. 2 Treatment of cell lines with nomlabofusp leads to cellular entry and increased FXN levels in mitochondria. (**a**) Rat H9c2 cells were exposed to 10 μM nomlabofusp or vehicle for 3 days. 24 h after the last dose, cells were trypsinized to remove non-internalized nomlabofusp and seeded onto an imaging plate. After a 24-h recovery, cells were fixed, stained with a human-specific FXN antibody, Tomm20 antibody, and Hoechst 33,342, then imaged by confocal microscopy. White arrows highlight mitochondrial localization of human FXN in the merge panel, and identical locations in the FXN and Tomm20 panels. Scale bar = 10 μm (**b**) H9c2 cells were exposed to 10 μM nomlabofusp or vehicle for 3 days. One day after the last exposure, cells were trypsinized to remove non-internalized nomlabofusp and re-seeded in a cell culture flask. After a 24-h recovery, cells were harvested, and mitochondria isolated. Whole cell extracts, mitochondrial fractions, and post-mitochondrial ("cytoplasmic") supernatants were separated by SDS-PAGE and analyzed by western blotting. (**c**) same as **a**, except in human SH-SY5Y cells. Acquisition settings were used such that the endogenous human FXN signal was barely detectable in the vehicle treated cells, ensuring that the observed FXN signal was a result of nomlabofusp delivery. (**d**) same as **b**, except in SH-SY5Y cells. (**e**) Mouse C2C12 cells, either FXN knockdown or scramble controls, were exposed to 10 μM or 20 μM nomlabofusp or vehicle for 3 days. 24 h after the last dose, cells were trypsinized to remove non-internalized nomlabofusp and harvested. Cell extracts were separated by SDS-PAGE and analyzed by western blotting. (**f**) Same as **e**, except in human HEK293-derived cells

after nomlabofusp exposure, both as analyzed by whole cell extracts and in the mitochondrial fraction (Fig. 2d).

To ensure that the existing levels of endogenous FXN did not affect nomlabofusp uptake and mitochondrial import, we also established stable FXN knockdown cell lines (and corresponding scramble control cell lines) in mouse C2C12 cells and human HEK293 cells to create cells that had low levels of FXN, analogous to what occurs in patients with FRDA. Exposure to nomlabofusp in both the knockdown and control cells resulted in a dose-dependent increase in mature human FXN (Fig. 2e and f). Thus, nomlabofusp exposure increased mature human FXN protein levels in these cells irrespective of the level of endogenous mouse or human FXN. Together, these data demonstrate that nomlabofusp penetrates cells, is imported into mitochondria and processed to mature FXN, and increases human FXN protein levels in these cells.

Increase in FXN Levels in Buccal Cells From Study Subjects with FRDA after Nomlabofusp Exposure

In a Phase 1, double-blind, placebo-controlled MAD study of nomlabofusp administration in adults with FRDA, a dose-dependent increase in FXN concentrations in skin and buccal cells (14) was observed after treatment with nomlabofusp. As shown in Fig. 3a, an increase in FXN levels in buccal cells was observed after 13 days of daily dosing of 3 subjects with 100 mg nomlabofusp, with levels returning to baseline 9 days after the completion of the treatment period. Considering the relatively short half-life of nomlabofusp this decrease in FXN over several days after cessation of dosing is not unexpected. A mean FXN increase of 4.7-fold was noted at Day 13 of treatment compared to baseline in these 3 subjects (4.5-, 3.6- and 6.1-fold individually). Western blot analysis was performed on the buccal cell homogenates to evaluate whether the observed increased levels of FXN after nomlabofusp treatment were processed to mFXN. Due to lower sensitivity of western blot method compared to the LC–MS/MS, as well as the relatively low protein concentration obtained from buccal cell homogenates, the homogenates from three subjects with FRDA treated with nomlabofusp were pooled, and FXN immunoprecipitated using an antibody that recognizes both endogenous FXN and full length nomlabofusp (Fig. 3b). As explained in Materials and Methods, only 3 patients' samples were eligible and had to be pooled for this analysis. Mature (~ 14 kDa) FXN was robustly immunoprecipitated from the NHV sample and could still be detected when a fourfold dilution of the sample was analyzed, approximating the FXN levels expected in patients with FRDA. The mature FXN signal in the pooled baseline samples from study subjects with FRDA was lower than the fourfold diluted NHV sample, but still detectable. Strikingly, the signal for mature FXN increased in the samples from FRDA subjects after 13 days of daily dosing with nomlabofusp. This is consistent with the previous report using the hybrid LC–MS/MS method that showed peptides corresponding to mature FXN, but not those specific for nomlabofusp, increased in tissue samples after nomlabofusp treatment (14). Furthermore,

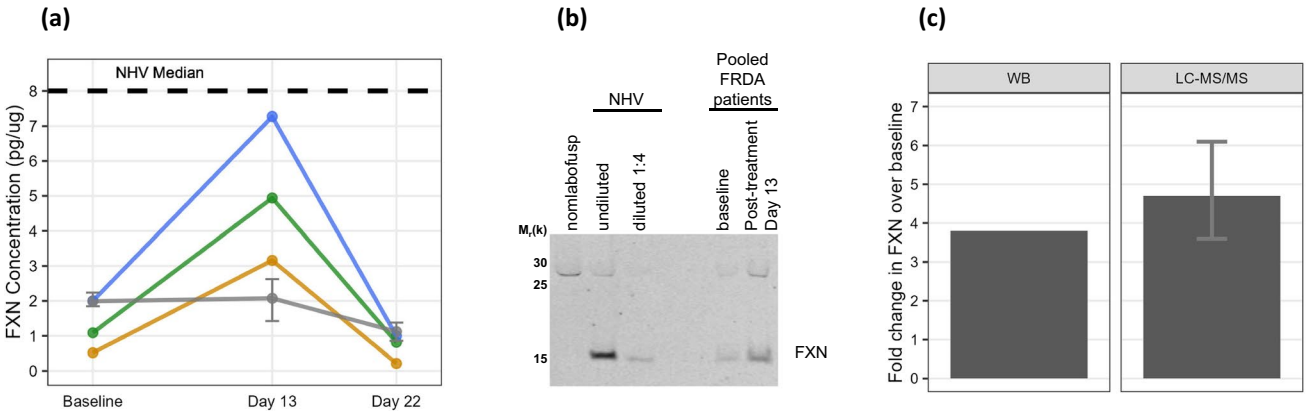

Fig. 3 Increase in FXN levels in buccal cells from study subjects with FRDA after nomlabofusp treatment. (**a**) FXN concentrations measured by LC–MS/MS in buccal tissue samples from 3 study subjects with FRDA, before and after dosing with 100 mg nomlabofusp. Individual subjects are shown in blue, green and gold; placebo group is shown in gray with median and interquartile range. The median tissue FXN concentration of 8.002 pg/µg taken from 60 NHVs is shown as the black dashed line (**b**) Increase in mature FXN in buccal cells from pooled samples taken from study subjects with FRDA after administration of 100 mg nomlabofusp for 13 days, measured via FXN immunoprecipitation (**c**) Comparison of western blot (WB) and hybrid LC–MS/MS methods for fold-change in FXN levels after treatment compared to baseline levels are shown. The WB histogram represents the pooled sample from 3 study subjects, whereas the LC–MS/MS histogram represents the mean of the 3 samples tested individually with the error bars showing the maximum and minimum values

a semi-quantitative densitometric measurement (relative light units) of the bands in the western blot indicated that the increase in FXN after dosing was comparable to that shown by the LC–MS/MS method (Fig. 3c), providing evidence that most, if not all, of the change from baseline in nomlabofusp concentration detected by the LC–MS/MS method is accounted for by mFXN. A ~ 25–30 kDa band was seen in the NHV sample, who were not dosed with nomlabofusp; considering the small size of TAT, this band likely represents endogenous immature MTS-FXN, which is not easily differentiated from nomlabofusp on a western blot.

Changes in Gene Expression in Buccal Cells from Study Subjects with FRDA after Nomlabofusp Treatment

Several studies have reported changes in gene expression correlating with changes in FXN levels in FRDA models and samples from patients with FRDA (25–27). As no molecular biomarkers have been identified for FRDA to monitor disease progression or evaluate treatment efficacy, we sought to evaluate gene expression. Using preliminary studies examining gene expression changes in a FRDA mouse model, various cell models (data not shown), and published data, we identified 243 genes to examine as potential FRDA biomarkers from buccal cell samples from patients with FRDA. Using nCounter® (Nanostring Technologies), gene expression was measured in buccal cells collected from study subjects in a Phase 1 MAD study (NCT04519567, (14)). In Fig. 4 data from the three study subjects with FRDA, corresponding to the western blot samples, are shown for BTG2, EGR1, SOD2, and XPO6. Median gene expression values from NHV controls (58 samples taken at multiple time points from 10 subjects) are shown as a dashed black line for reference. For each of the genes shown, the expression level in study subjects with FRDA at baseline was lower compared with what was observed in NHVs, confirming that the effect of low FXN levels on gene transcription can be observed in buccal cells. A notable change in gene expression was observed in subjects with FRDA who received nomlabofusp compared with those who received placebo, indicating intracellular pharmacodynamic activity. Additionally, gene expression in these subjects treated with nomlabofusp trended in the direction of NHV controls, while those who received placebo did not, demonstrating that the restoration of FXN levels may restore FXN function. Interestingly, it appeared that gene expression generally did not change much until after the conclusion of the treatment period on Day 13, increased over a week later at Day 22, and then was sustained in 2 subjects at Day 43. The relevance of the timing of the observed modulation is unknown.

Discussion

With the establishment of FXN deficiency as the pathophysiological cause of FRDA (5), it is rational to hypothesize that FXN replacement should revert the functional deficits caused by the inherent FXN deficiency in patients with FRDA. Hence, nomlabofusp was designed specifically to enter cells using it's TAT-cell penetrant peptide (28), after which its endogenous MTS sequence would enable import into the mitochondrial matrix (29). There it is expected to be processed via cleavage by MPP (30) into mFXN. The removal of TAT-MTS as a result of this processing also prevents any potential CPP-mediated exit of nomlabofusp from mitochondria (31). Hence, the exogenously introduced mFXN would remain resident within the mitochondrial matrix, undifferentiated in structure, function and disposition from endogenous mFXN. In this article we provided evidence for the proposed mechanism of action of nomlabofusp using several cell lines *in vitro*, and in buccal epithelial cells from treated patients.

Due to its genetic etiology FXN deficiency exists in all organs, tissues and cells of a patient with FRDA. However, there are some particularly vulnerable organs that develop severe clinical pathology in FRDA, including (a) the nervous system, primarily dorsal root ganglia, spinal cord, cerebellum and peripheral nerves (b) the heart muscle, and (c) the skeletal system, primarily the spine and feet. Therefore, we chose 4 different but relevant cell lines to develop evidence for the proposed mechanism of action of nomlabofusp. H9c2 myoblast cells, which are derived from rat embryonic heart tissue and exhibit properties of both cardiac and skeletal muscle depending upon the culture conditions and differentiation state (32). SH-SY5Y human neuroblastoma cells exhibit a neuroblast-like morphology with non-polarized cell bodies and few, truncated, processes (33), and express both adrenergic and dopaminergic markers (34). C2C12 myoblast cells are derived from mouse thigh skeletal muscle and are widely used in biomedical research, particularly for studying muscle biology (35). HEK293 cells, derived from human embryonic kidney tissue, exhibit an epithelial-like phenotype (36) as well as properties of immature neurons (37). Exposure to nomlabofusp during culture led to cellular uptake, mitochondrial localization and processing into mature human frataxin.

For tissue sampling in humans, because the primary target tissues of FRDA such as heart and brain are difficult to sample, the use of peripheral tissues such as buccal cells to assess FXN levels has been a well-established practical alternative (4, 38). Buccal swabs can be easily, painlessly, and repeatedly collected from patients, and FXN levels in buccal swabs correlate with FXN levels in other tissues

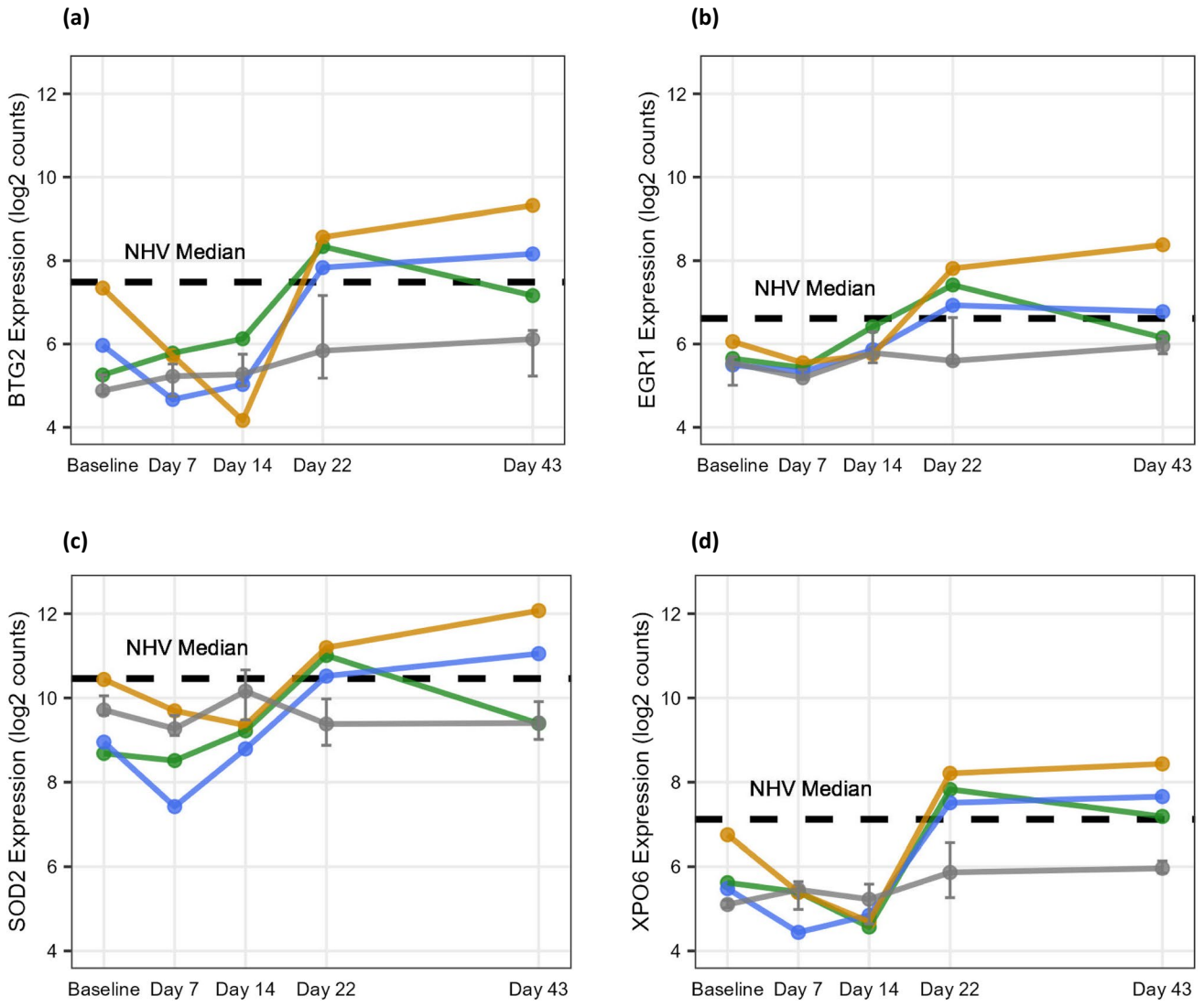

Fig. 4 Pharmacodynamic changes in gene expression in buccal cells from study subjects with FRDA after nomlabofusp treatment. mRNA expression of (**a**) BTG2, (**b**) EGR1, (**c**) SOD2, (**d**) XPO6 in buccal cells from study subjects with FRDA before treatment (baseline) and after 100 mg nomlabofusp treatment (Days 7, 14, 22 and 43). Individual subjects are shown in blue, green and gold; placebo group (7 subjects) is shown in gray with median and interquartile range. The median gene expression value from NHVs (58 samples taken at multiple time points from 10 NHVs) is shown as the black dashed line

(3). Hence, we collected buccal swab tissue samples from patients with FRDA and NHV controls to attain evidence of nomlabofusp cellular and mitochondrial entry, processing, and pharmacodynamic activity. In samples obtained from adults with FRDA participating in a Phase 1 nomlabofusp clinical study, increases in levels of mitochondrial-localized, mature FXN was observed after treatment with nomlabofusp, consistent with our *in vitro* findings across multiple cell types. By virtue of TAT-mediated cell penetration utilizing endocytic pathways (20–22), some nomlabofusp remained in internal punctate compartments – likely endocytic compartments. Additionally, nomlabofusp was detected in the nucleus of treated cells, consistent with a tendency of TAT and TAT-fusion proteins to localize to the nucleus (24, 39, 40). However, due to the presence of the endogenous MTS sequence attached to FXN, some nomlabofusp was also imported into mitochondria, consistent with the fact that most mitochondrial proteins are translated on cytoplasmic ribosomes before being imported into mitochondria. Once imported, the TAT plus MTS portion of nomlabofusp is cleaved by MPP (15, 30, 41), resulting in mFXN within the mitochondrial matrix that is indistinguishable from endogenous FXN. This MPP-mediated cleavage event provides a simple method to monitor mitochondrial, rather than simply whole cellular, increases in FXN protein after nomlabofusp treatment. As

the mitochondrial and cytoplasmic subcellular fractionation experiments had demonstrated, mFXN (~ 14 kDa) was only present inside mitochondria in the cells studied.

Even though a correlation between tissue FXN concentrations and the rate of change in the Friedreich's Ataxia Rating Scale (FARS) has been demonstrated (3), to date, no molecular biomarkers have been validated to either monitor disease progression or evaluate treatment effect in patients with FRDA. The current best practice, the modified FARS, requires both patient input and clinician interpretation, is vulnerable to subjectivity and variability, has shown significant placebo effects (42) and requires a year or more to show any detectable treatment effect. Also, the measurement of functional cellular activity such as succinate dehydrogenase or aconitase activity in peripheral tissues, e.g., buccal or skin cells, is confronted by technical infeasibilities. To circumvent these challenges, we studied transcriptomics in patients with FRDA. Several studies have reported changes in gene expression in patients with FRDA and animal models (25–27, 43, 44). Changes in gene expression have also been observed in tissues from patients with other mitochondrial diseases (45) suggesting that these changes in transcription may, in part, represent cellular regulation of metabolic, and/or signaling pathways to best optimize cellular function (46). Here, we investigated gene expression in buccal cells – an easily accessible peripheral tissue that could be sampled multiple times throughout the short time course of the clinical trial. We exemplify four genes, BTG2, EGR1, SOD2, and XPO6, that we discovered to be expressed at lower levels in patients with FRDA compared to NHVs.

BTG2 (B-cell translocation gene 2) is also known as nerve growth factor inducible anti-proliferative protein PC3. It is a protein that plays important roles in several biological processes including cell-cycle progression, induction of cellular senescence, cellular differentiation including neurogenesis, hematopoiesis, and integrated stress responses such as the response against oxidative stress (47–49). EGR1 (early growth response 1) is also known as nerve growth factor-induced protein A. It is a transcription factor that is a major mediator and regulator of synaptic plasticity and neuronal activity in both physiological and pathological conditions (50). EGR1 is involved in the development, homeostasis, and healing processes of various connective tissues, such as tendon, cartilage and bone, and adipose tissue, mainly via the regulation of extracellular matrix (51). Its expression is closely associated with neuronal activity and processes such as learning and memory (52). SOD2 (superoxide dismutase 2) is also known as mitochondrial superoxide dismutase or manganese superoxide dismutase. It is critical for preventing mitochondrial dysfunction and cell death resulting from oxidative stress, maintaining normal tissue homeostasis and supporting embryonic development. Interestingly, SOD2 mRNA level has been shown to positively correlate with FXN mRNA transcription in the FRDA YG8R mouse model (53). It was previously shown that SOD2 levels were lower in fibroblasts from patients with FRDA compared fibroblasts from NHVs, and that cells from patients with FRDA showed an impaired ability to upregulate SOD2 expression in response to oxidative stress (54). SOD2 downregulation in skeletal muscle from patients with FRDA was more recently published as well (55). XPO6 (Exportin-6), belongs to the exportin family and plays a crucial role in nuclear export processes. XPO6 primarily mediates the nuclear export of actin and profilin-actin complexes in somatic cells and has been implicated in cellular senescence (56). More recently, XPO6 upregulation has been noted in multiple cancers (57), in a chronic obstructive pulmonary disease mouse model (58), and in a pig model of donation after circulatory death (59). Nevertheless, the role of XPO6 in disease mechanisms remains unclear to date.

For all four genes, after administration of nomlabofusp to adults with FRDA an increase in gene expression was noted that approached gene expression measured in cells from NHVs. Along with increases in gene expression, increases in tissue FXN concentrations were observed in adults with FRDA after administration of nomlabofusp, suggesting that the FXN delivered by nomlabofusp was pharmacodynamically active. Because the changes in gene expression were observed 9 days after nomlabofusp dosing completed, and in many cases persisted 30 days after dosing completion, we interpreted these observations to mean that these changes are indirect and relatively downstream of FXN itself and indicate the lasting effect of an acute increase in FXN levels. The clinical relevance of the observed changes in gene expression after treatment with nomlabofusp relative to FRDA causation or pathology requires further investigation and remains an area of active research for us.

Conclusion

In conclusion, we have demonstrated that nomlabofusp successfully translocates into cells and thereafter into mitochondria where it is processed into mature and active FXN that is indistinguishable from endogenous FXN. We have also observed increases in tissue FXN concentrations in adult FRDA subjects treated with nomlabofusp that appears to be pharmacodynamically active as evidenced by observed changes in the expression of certain genes. Demonstration of increased mFXN levels within mitochondria in multiple cell lines (H9c2, SH-SY5Y, C2C12, HEK293) derived from multiple cell types and species after exposure to nomlabofusp provides evidence confirming the nonspecific, body-wide tissue penetration of the TAT-based cell penetration mechanism. Collectively, these findings support the potential for FXN replacement therapy with nomlabofusp to modify the

disease course of FRDA by increasing tissue FXN concentrations in the mitochondria of many tissues and cell types in patients with FRDA.

Acknowledgements The methodologies applied in these studies were adapted from initial techniques developed in our laboratory by prior employees Dr. David Bettoun, Ms. Apeksha Khatiwada and Mr. Devin Schecter. The authors thank the following individuals for their comprehensive review of this manuscript: Dr. Flavia De Toni, Dr. Vanessa Ragaglia, Dr. Rusty Clayton, Dr. Carole Ben-Maimon and Mrs. Jennifer Johansson.

Author Contributions Conceptualization: MGB, GS.
Data Curation: MGB, JJ, NS.
Formal Analysis: MGB, JJ, NS.
Investigation: MGB, GS.
Methodology: MGB, JJ, NS.
Resources: GS.
Visualization: MGB, JJ, NS.
Supervision: GS.
Validation: MGB, JJ.
Writing – original draft: MGB, JJ, NS, GS.
Writing – review & editing: GS.

Funding This research was funded by Larimar Therapeutics, Inc.

Declarations

Conflict of Interest MGB, JJ, NS and GS are employed by Larimar Therapeutics, Inc. and they and/or their immediate family members may hold company stock or stock options. GS chairs the Larimar Scientific Advisory Board.

References

1. Delatycki MB, Corben LA. Clinical features of Friedreich ataxia. J Child Neurol. 2012;27(9):1133–7. https://doi.org/10.1177/0883073812448230.
2. Lynch DR, Schadt K, Kichula E, McCormack S, Lin KY. Friedreich ataxia: multidisciplinary clinical care. J Multidiscip Healthc. 2021;14:1645–58. https://doi.org/10.2147/JMDH.S292945.
3. Plasterer HL, Deutsch EC, Belmonte M, Egan E, Lynch DR, Rusche JR. Development of Frataxin gene expression measures for the evaluation of experimental treatments in Friedreich's ataxia. PLoS ONE. 2013;8(5):e63958. https://doi.org/10.1371/journal.pone.0063958.
4. Deutsch EC, Santani AB, Perlman SL, Farmer JM, Stolle CA, Marusich MF, *et al*. A rapid, noninvasive immunoassay for frataxin: utility in assessment of Friedreich ataxia. Mol Genet Metab. 2010;101(2–3):238–45. https://doi.org/10.1016/j.ymgme.2010.07.001.
5. Pandolfo M. Friedreich ataxia. Arch Neurol. 2008;75(10):1296–303.
6. Marmolino D. Friedreich's ataxia: past, present and future. Brain Res Rev. 2011;67(1–2):311–30. https://doi.org/10.1016/j.brainresrev.2011.04.001.
7. Campuzano V, Montermini L, Lutz Y, Cova L, Hindelang C, Jiralerspong S, *et al*. Frataxin is reduced in Friedreich ataxia patients and is associated with mitochondrial membranes. Hum Mol Genet. 1997;6(11):1771–80. https://doi.org/10.1093/hmg/6.11.1771.
8. Gibson TJ, Koonin EV, Musco G, Pastore A, Bork P. Friedreich's ataxia protein: phylogenetic evidence for mitochondrial dysfunction. Trends Neurosci. 1996;19(11):465–8. https://doi.org/10.1016/S0166-2236(96)20054-2.
9. Zhang Y, Lyver ER, Knight SA, Pain D, Lesuisse E, Dancis A. Mrs3p, Mrs4p, and frataxin provide iron for Fe-S cluster synthesis in mitochondria. J Biol Chem. 2006;281(32):22493–502. https://doi.org/10.1074/jbc.M604246200.
10. Rotig A, de Lonlay P, Chretien D, Foury F, Koenig M, Sidi D, *et al*. Aconitase and mitochondrial iron-sulphur protein deficiency in Friedreich ataxia. Nat Genet. 1997;17(2):215–7. https://doi.org/10.1038/ng1097-215.
11. Albracht SP. The prosthetic groups in succinate dehydrogenase. Number and stoichiometry. Biochim Biophys Acta. 1980;612(1):11–28. https://doi.org/10.1016/0005-2744(80)90274-0.
12. Ye H, Rouault TA. Human iron-sulfur cluster assembly, cellular iron homeostasis, and disease. Biochemistry. 2010;49(24):4945–56. https://doi.org/10.1021/bi1004798.
13. Sarko D, Beijer B, Garcia Boy R, Nothelfer E-M, Leotta K, Eisenhut M, *et al*. The pharmacokinetics of cell-penetrating peptides. Mol Pharm. 2010;7(6):2224–31. https://doi.org/10.1021/mp100223d.
14. Clayton R, Galas T, Scherer N, Farmer J, Ruiz N, Hamdani M, *et al*. Safety, pharmacokinetics, and pharmacodynamics of nomlabofusp (CTI-1601) in Friedreich's ataxia. Ann Clin Transl Neurol. 2024;11(3):540–53. https://doi.org/10.1002/acn3.51971.
15. Vyas PM, Tomamichel WJ, Pride PM, Babbey CM, Wang Q, Mercier J, *et al*. A TAT-frataxin fusion protein increases lifespan and cardiac function in a conditional Friedreich's ataxia mouse model. Hum Mol Genet. 2012;21(6):1230–47. https://doi.org/10.1093/hmg/ddr554.
16. Palmer CS, Anderson AJ, Stojanovski D. Mitochondrial protein import dysfunction: mitochondrial disease, neurodegenerative disease and cancer. FEBS Lett. 2021;595(8):1107–31. https://doi.org/10.1002/1873-3468.14022.
17. Stehling O, Elsasser HP, Bruckel B, Muhlenhoff U, Lill R. Iron-sulfur protein maturation in human cells: evidence for a function of frataxin. Hum Mol Genet. 2004;13(23):3007–15. https://doi.org/10.1093/hmg/ddh324.
18. Bullard JH, Purdom E, Hansen KD, Dudoit S. Evaluation of statistical methods for normalization and differential expression in mRNA-Seq experiments. BMC Bioinformatics. 2010;11:94. https://doi.org/10.1186/1471-2105-11-94.
19. Risso D, Ngai J, Speed TP, Dudoit S. Normalization of RNA-seq data using factor analysis of control genes or samples. Nat Biotechnol. 2014;32(9):896–902. https://doi.org/10.1038/nbt.2931.
20. Wadia JS, Stan RV, Dowdy SF. Transducible TAT-HA fusogenic peptide enhances escape of TAT-fusion proteins after lipid raft macropinocytosis. Nat Med. 2004;10(3):310–5. https://doi.org/10.1038/nm996.
21. Fittipaldi A, Ferrari A, Zoppe M, Arcangeli C, Pellegrini V, Beltram F, *et al*. Cell membrane lipid rafts mediate

caveolar endocytosis of HIV-1 Tat fusion proteins. J Biol Chem. 2003;278(36):34141–9. https://doi.org/10.1074/jbc.M303045200.
22. Ferrari A, Pellegrini V, Arcangeli C, Fittipaldi A, Giacca M, Beltram F. Caveolae-mediated internalization of extracellular HIV-1 tat fusion proteins visualized in real time. Mol Ther. 2003;8(2):284–94. https://doi.org/10.1016/s1525-0016(03)00122-9.
23. Richard JP, Melikov K, Brooks H, Prevot P, Lebleu B, Chernomordik LV. Cellular uptake of unconjugated TAT peptide involves clathrin-dependent endocytosis and heparan sulfate receptors. J Biol Chem. 2005;280(15):15300–6. https://doi.org/10.1074/jbc.M401604200.
24. Vives E, Brodin P, Lebleu B. A truncated HIV-1 Tat protein basic domain rapidly translocates through the plasma membrane and accumulates in the cell nucleus. J Biol Chem. 1997;272(25):16010–7. https://doi.org/10.1074/jbc.272.25.16010.
25. Napierala JS, Li Y, Lu Y, Lin K, Hauser LA, Lynch DR, *et al*. Comprehensive analysis of gene expression patterns in Friedreich's ataxia fibroblasts by RNA sequencing reveals altered levels of protein synthesis factors and solute carriers. Dis Model Mech. 2017;10(11):1353–69. https://doi.org/10.1242/dmm.030536.
26. McMackin MZ, Durbin-Johnson B, Napierala M, Napierala JS, Ruiz L, Napoli E, *et al*. Potential biomarker identification for Friedreich's ataxia using overlapping gene expression patterns in patient cells and mouse dorsal root ganglion. PLoS ONE. 2019;14(10):e0223209. https://doi.org/10.1371/journal.pone.0223209.
27. Huang ML, Sivagurunathan S, Ting S, Jansson PJ, Austin CJ, Kelly M, *et al*. Molecular and functional alterations in a mouse cardiac model of Friedreich ataxia: activation of the integrated stress response, eIF2alpha phosphorylation, and the induction of downstream targets. Am J Pathol. 2013;183(3):745–57. https://doi.org/10.1016/j.ajpath.2013.05.032.
28. Derakhshankhah H, Jafari S. Cell penetrating peptides: A concise review with emphasis on biomedical applications. Biomed Pharmacother. 2018;108:1090–6. https://doi.org/10.1016/j.biopha.2018.09.097.
29. Omura T. Mitochondria-targeting sequence, a multi-role sorting sequence recognized at all steps of protein import into mitochondria. J Biochem. 1998;123(6):1010–6. https://doi.org/10.1093/oxfordjournals.jbchem.a022036.
30. Gakh O, Cavadini P, Isaya G. Mitochondrial processing peptidases. Biochim Biophys Acta. 2002;1592(1):63–77. https://doi.org/10.1016/s0167-4889(02)00265-3.
31. Del Gaizo V, Payne RM. A novel TAT–Mitochondrial signal sequence fusion protein is processed, stays in mitochondria, and crosses the placenta. Mol Ther. 2003;7(6):720–30. https://doi.org/10.1016/s1525-0016(03)00130-8.
32. Branco AF, Pereira SP, Gonzalez S, Gusev O, Rizvanov AA, Oliveira PJ. Gene expression profiling of H9c2 myoblast differentiation towards a cardiac-like phenotype. PLoS ONE. 2015;10(6):e0129303. https://doi.org/10.1371/journal.pone.0129303.
33. Kovalevich J, Langford D. Considerations for the use of SH-SY5Y neuroblastoma cells in neurobiology. Methods Mol Biol. 2013;1078:9–21. https://doi.org/10.1007/978-1-62703-640-5_2.
34. Kaya ZB, Santiago-Padilla V, Lim M, Boschen SL, Atilla P, McLean PJ. Optimizing SH-SY5Y cell culture: exploring the beneficial effects of an alternative media supplement on cell proliferation and viability. Sci Rep. 2024;14(1):4775. https://doi.org/10.1038/s41598-024-55516-5.
35. Katagiri T, Yamaguchi A, Komaki M, Abe E, Takahashi N, Ikeda T, *et al*. Bone morphogenetic protein-2 converts the differentiation pathway of C2C12 myoblasts into the osteoblast lineage. J Cell Biol. 1994;127(6 Pt 1):1755–66. https://doi.org/10.1083/jcb.127.6.1755.
36. Thomas P, Smart TG. HEK293 cell line: a vehicle for the expression of recombinant proteins. J Pharmacol Toxicol Methods. 2005;51(3):187–200. https://doi.org/10.1016/j.vascn.2004.08.014.
37. Gordon J, Amini S. General overview of neuronal cell culture. Methods Mol Biol. 2021;2311:1–8. https://doi.org/10.1007/978-1-0716-1437-2_1.
38. Lazaropoulos M, Dong Y, Clark E, Greeley NR, Seyer LA, Brigatti KW, *et al*. Frataxin levels in peripheral tissue in Friedreich ataxia. Ann Clin Transl Neurol. 2015;2(8):831–42. https://doi.org/10.1002/acn3.225.
39. Hauber J, Perkins A, Heimer EP, Cullen BR. Trans-activation of human immunodeficiency virus gene expression is mediated by nuclear events. Proc Natl Acad Sci U S A. 1987;84(18):6364–8. https://doi.org/10.1073/pnas.84.18.6364.
40. Mann DA, Frankel AD. Endocytosis and targeting of exogenous HIV-1 Tat protein. EMBO J. 1991;10(7):1733–9. https://doi.org/10.1002/j.1460-2075.1991.tb07697.x.
41 Cavadini P, Adamec J, Taroni F, Gakh O, Isaya G. Two-step processing of human frataxin by mitochondrial processing peptidase. Precursor and intermediate forms are cleaved at different rates. J Biol Chem. 2000;275(52):41469–75. https://doi.org/10.1074/jbc.M006539200.
42. Lynch DR, Chin MP, Delatycki MB, Subramony SH, Corti M, Hoyle JC, *et al*. Safety and efficacy of omaveloxolone in Friedreich Ataxia (MOXIe Study). Ann Neurol. 2021;89(2):212–25. https://doi.org/10.1002/ana.25934.
43. Nachun D, Gao F, Isaacs C, Strawser C, Yang Z, Dokuru D, *et al*. Peripheral blood gene expression reveals an inflammatory transcriptomic signature in Friedreich's ataxia patients. Hum Mol Genet. 2018;27(17):2965–77. https://doi.org/10.1093/hmg/ddy198.
44. Angulo MB, Bertalovitz A, Argenziano MA, Yang J, Patel A, Zesiewicz T, *et al*. Frataxin deficiency alters gene expression in Friedreich ataxia derived IPSC-neurons and cardiomyocytes. Mol Genet Genomic Med. 2023;11(1):e2093. https://doi.org/10.1002/mgg3.2093.
45. Heddi A, Stepien G, Benke PJ, Wallace DC. Coordinate induction of energy gene expression in tissues of mitochondrial disease patients. J Biol Chem. 1999;274(33):22968–76. https://doi.org/10.1074/jbc.274.33.22968.
46. Eisenberg-Bord M, Schuldiner M. Ground control to major TOM: mitochondria-nucleus communication. FEBS J. 2017;284(2):196–210. https://doi.org/10.1111/febs.13778.
47. Miyata S, Mori Y, Tohyama M. PRMT1 and Btg2 regulates neurite outgrowth of Neuro2a cells. Neurosci Lett. 2008;445(2):162–5. https://doi.org/10.1016/j.neulet.2008.08.065.
48. Kim SH, Jung IR, Hwang SS. Emerging role of anti-proliferative protein BTG1 and BTG2. BMB Rep. 2022;55(8):380–8. https://doi.org/10.5483/BMBRep.2022.55.8.092.
49. Karve TM, Rosen EM. B-cell translocation gene 2 (BTG2) stimulates cellular antioxidant defenses through the antioxidant transcription factor NFE2L2 in human mammary epithelial cells. J Biol Chem. 2012;287(37):31503–14. https://doi.org/10.1074/jbc.M112.367433.
50. Duclot F, Kabbaj M. The Role of Early Growth Response 1 (EGR1) in Brain Plasticity and Neuropsychiatric Disorders. Front Behav Neurosci. 2017;11:35. https://doi.org/10.3389/fnbeh.2017.00035.
51. Havis E, Duprez D. EGR1 transcription factor is a multifaceted regulator of matrix production in tendons and other connective tissues. Int J Mol Sci. 2020;21(5):1664. https://doi.org/10.3390/ijms21051664.
52. Veyrac A, Besnard A, Caboche J, Davis S, Laroche S. The transcription factor Zif268/Egr1, brain plasticity, and memory. Prog

Mol Biol Transl Sci. 2014;122:89–129. https://doi.org/10.1016/B978-0-12-420170-5.00004-0.
53. Shan Y, Schoenfeld RA, Hayashi G, Napoli E, Akiyama T, Iodi Carstens M, *et al*. Frataxin deficiency leads to defects in expression of antioxidants and Nrf2 expression in dorsal root ganglia of the Friedreich's ataxia YG8R mouse model. Antioxid Redox Signal. 2013;19(13):1481–93. https://doi.org/10.1089/ars.2012.4537.
54. Marmolino D, Manto M, Acquaviva F, Vergara P, Ravella A, Monticelli A, *et al*. PGC-1alpha down-regulation affects the antioxidant response in Friedreich's ataxia. PLoS ONE. 2010;5(4):e10025. https://doi.org/10.1371/journal.pone.0010025.
55. Indelicato E, Faserl K, Amprosi M, Nachbauer W, Schneider R, Wanschitz J, *et al*. Skeletal muscle proteome analysis underpins multifaceted mitochondrial dysfunction in Friedreich's ataxia. Front Neurosci. 2023;17:1289027. https://doi.org/10.3389/fnins.2023.1289027.
56. Park SH, Park TJ, Lim IK. Reduction of exportin 6 activity leads to actin accumulation via failure of RanGTP restoration and NTF2 sequestration in the nuclei of senescent cells. Exp Cell Res. 2011;317(7):941–54. https://doi.org/10.1016/j.yexcr.2010.12.023.
57. Zhu C, Kim SJ, Mooradian A, Wang F, Li Z, Holohan S, *et al*. Cancer-associated exportin-6 upregulation inhibits the transcriptionally repressive and anticancer effects of nuclear profilin-1. Cell Rep. 2021;34(7):108749. https://doi.org/10.1016/j.celrep.2021.108749.
58. Wu Y, Gou Y, Wang T, Li P, Li Y, Lu X, *et al*. Exportin XPO6 upregulation activates the TLR2/MyD88/NF-kappaB signaling by facilitating TLR2 mRNA nuclear export in COPD pulmonary monocytes. Int Immunopharmacol. 2024;135:112310. https://doi.org/10.1016/j.intimp.2024.112310.
59. Saemann L, Wachter K, Georgevici AI, Pohl S, Hoorn F, Veres G, *et al*. Transcriptomic changes in the myocardium and coronary artery of donation after circulatory death hearts following ex vivo machine perfusion. Int J Mol Sci. 2024;25(2):1261. https://doi.org/10.3390/ijms25021261.